Stem Cells, 2025, **43**, sxaf010
https://doi.org/10.1093/stmcls/sxaf010
Advance access publication 19 March 2025
Original Research

SARS-CoV2 infection triggers inflammatory conditions and astrogliosis-related gene expression in long-term human cortical organoids

Mathilde Colinet[1], Ioana Chiver[1], Antonela Bonafina[1], Gérald Masset[1], Daniel Almansa[1], Emmanuel Di Valentin[2], Jean-Claude Twizere[3], Laurent Nguyen[1,4,‡,*], Ira Espuny-Camacho[1,5,‡,*]

[1]Laboratory of Molecular Regulation of Neurogenesis, GIGA Institute, University of Liège, Liège 4000, Belgium,
[2]GIGA Viral Vector Platform, GIGA Institute, University of Liège, Liège 4000, Belgium,
[3]Laboratory of Viral Interactomes, Unit of Molecular Biology of Diseases, GIGA Institute, University of Liège, Liège 4000, Belgium,
[4]WELBIO Department, WEL Research Institute, Wavre 1300, Belgium
[5]GIGA HIPS, GIGA Institute, University of Liège, Liège 4000, Belgium

[*]Corresponding authors: Laurent Nguyen, GIGA Institute, University of Liège, Liège 400, Belgium. E-mail: (lnguyen@uliege.be, im.espunycamacho@uliege.be); Ira Espuny-Camacho, GIGA Institute, University of Liège, Liège 4000, Belgium. E-mail: im.espunycamacho@uliege.be)
[‡]Co-last authors.

Abstract

SARS-CoV2, severe acute respiratory syndrome coronavirus 2, is frequently associated with neurological manifestations. Despite the presence of mild to severe CNS-related symptoms in a cohort of patients, there is no consensus whether the virus can infect directly brain tissue or if the symptoms in patients are a consequence of peripheral infectivity of the virus. Here, we use long-term human stem cell-derived cortical organoids to assess SARS-CoV2 infectivity of brain cells and unravel the cell-type tropism and its downstream pathological effects. Our results show consistent and reproducible low levels of SARS-CoV2 infection of astrocytes, deep projection neurons, upper callosal neurons, and inhibitory neurons in 6 months of human cortical organoids. Interestingly, astrocytes showed the highest infection rate among all infected cell populations which led to changes in their morphology and upregulation of SERPINA3, CD44, and S100A10 astrogliosis markers. Further, transcriptomic analysis revealed overall changes in expression of genes related to cell metabolism, astrogliosis and, inflammation and further, upregulation of cell survival pathways. Thus, local and minor infectivity of SARS-CoV2 in the brain may induce widespread adverse effects and lead to the resilience of dysregulated neurons and astrocytes within an inflammatory environment.

Key words: astrogliosis; human cortical organoids; inflammatory and cell survival mechanisms; SARS-CoV2 brain infectivity.

Received: 3 February 2024; Accepted: 18 February 2025.

Graphical Abstract

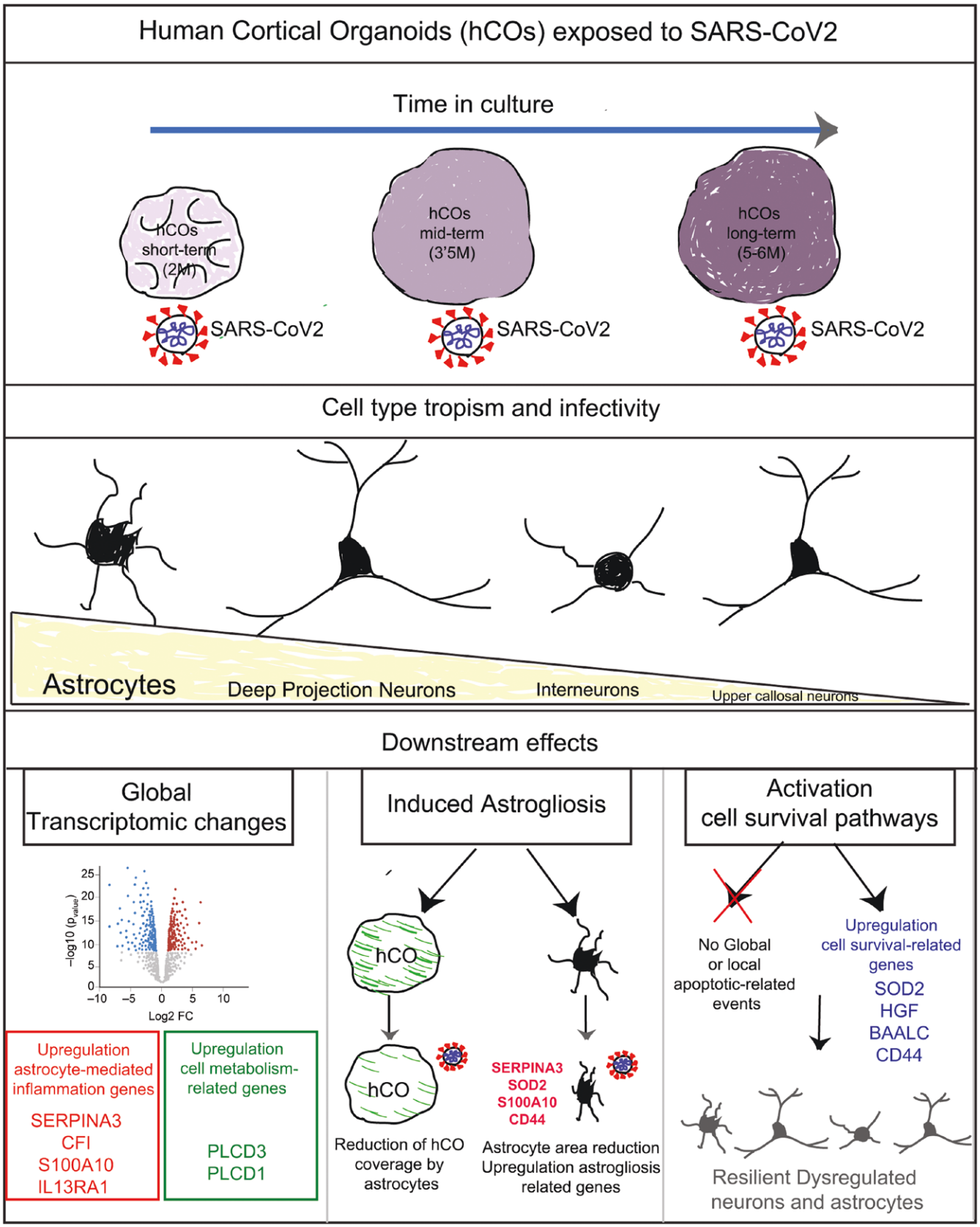

Significance statement

Neurological-related symptoms are present in a subset of coronavirus disease 2019 patients, however, it is not yet clear whether SARS-CoV2 can directly infect the human brain and which are the direct downstream effects. In this study, we show that SARS-CoV2 can infect at low levels astrocytes and neurons from long-term cultured human cortical organoids. SARS-CoV2 infection leads to astrogliosis and triggers global gene expression changes related to inflammation, cell metabolism, and cell survival. These findings suggest that SARS-CoV2 infection may lead to the appearance of resilient dysregulated astrocytes and neurons in the brain.

Introduction

SARS-CoV2, severe acute respiratory syndrome coronavirus 2, that causes coronavirus disease 2019 (COVID-19), is associated with a plethora of symptoms in patients ranging from mild fever to pneumonia and, in a small proportion of cases, systemic defects that can lead to the death of the individual.[1-4] Recent findings have associated SARS-CoV2-infectivity-related effects with alterations in multiple organs including lung, heart, kidney, and brain. While SARS-CoV2 mainly targets the respiratory system, neurological manifestations have also been detected in patients. These neurological adverse effects include anosmia, strokes, seizures, and impaired consciousness, among others.[5-8] Despite the observation of brain-related symptoms in a fraction of the patients, the analysis of postmortem brains or cerebral spinal fluid (CSF) samples from surviving patients has led to contradictory results with most reports failing to detect the presence of SARS-CoV2 particles.[9-13] These observations suggest either low levels of infection in brain tissue or on the contrary an absence of infectivity in the brain, where neurological-related effects would rely on SARS-CoV2 peripheral organ infection.

SARS-CoV2 viral entry has been proposed to be mediated by the binding of the virus spike S protein to the receptor angiotensin converting enzyme 2 (ACE2) in the target cell. This event is followed by the activation of the spike S protein upon cleavage enacted by the host proprotein convertase furin and by membrane-associated serine proteinases (MASPs),[14,15] which leads to the fusion of the virus membrane with the host cell membrane.[2,16] Whereas high levels of ACE2 expression have been detected in major target tissues of SARS-CoV2 infection such as lung, kidney, and heart, ACE2 levels are reported to be low or undetectable in the brain.[17] However, the expression of ACE2 co-receptors that potentiate SARS-CoV2 infectivity has been reported in several tissues, including the brain. These co-receptors include neuropilin 1 (NRP1) cell surface receptor,[16,18-20] dipeptidyl peptidase 4 (DPP4),[21] tyrosine-protein kinase receptor UFO (AXL),[22] extracellular matrix metalloproteinase inducer (CD147/BSG)[7,23,24] and endoplasmic reticulum (ER) stress-inducible chaperone BiP (GRP78/HSPA5).[25,26] These reports support the possibility that alternative receptors and co-receptors are mediating SARS-CoV2 entry in brain cells.

Concerning the downstream effects of SARS-CoV2 infectivity, recent reports performing multi-organ screenings by magnetic resonance imaging (MRI) have detected multiple anomalies in lungs and brain in a cohort of coronavirus disease 2019 (COVID-19) patients 6 months post-infection.[27] In addition, postmortem analysis of patient brain tissue has revealed broad cellular perturbations of most cell types by single-cell transcriptomic[28] and proteomic[9] analysis. These studies suggested the preferential infectivity of astrocyte glial cells and their consequent dysregulated homeostatic pathways linked to higher levels of inflammation detected in the brain. Whereas most studies have been focused on the adult brain, a recent report has shown hemorrhagic phenotypes in the cortex of human fetuses exposed to SARS-CoV2,[29] through a mechanism related to reduction in blood vessel integrity.[29-31] Several studies have used human pluripotent stem cell-derived brain organoids to analyze the infectivity of SARS-CoV2 in the brain and its pathological downstream effects. Infectivity of brain cell types has been reported to be low compared to the levels of infection detected for instance in models including choroid plexus epithelial and ependymal cells[32,33] and perivascular pericyte-like cells.[34] A few studies have corroborated in vitro the infectivity of astrocytes by SARS-CoV2 in agreement with the reports from postmortem brain sample analysis.[19,35] However, systematic studies analyzing the percentage of cells with different identities infected by the virus and their susceptibility to SARS-CoV2 infection in human cortical organoid models at different stages in vitro are currently missing.

Here, we analyze neural cell infectivity of SARS-CoV2 in human cortical organoid models to understand the cellular tropism of the virus at different brain organoid maturation stages. We found that astrocytes, deep projection neurons, upper callosal neurons, and inhibitory interneurons were infected by SARS-CoV2. Astrocytes showed the highest rate of infected cells among the specific cell population in human cortical organoids at late stages in vitro. We detected low levels of *ACE2* expression but higher levels of some of its co-receptors, including *NRP1*, *CD147*, *GRP78*, *NRP2,* and *AXL*, which may be involved in viral entry in the target cells. Mechanistically, we found that upon SARS-CoV2 infection, astrocytes undergo changes in morphology and upregulate SERPINA3, CD44, and S100A10 markers of astrogliosis, leading to broad adverse effects on cortical organoid cell populations by triggering an inflammatory response counteracted by upregulation of cell survival pathways.

Materials and methods

Human hCOs differentiation

Human cortical brain organoids (hCOs) were developed following a modified version of the Sasai lab protocol.[36] hESC-H9 cell line (WA09) (Metadata: Female, no disease-associated) acquired from Wicell was used under the approval from the ethical committee from the University of Liège: Comité d'Ethique Hospitalo-Facultaire Universitaire de Liège (707) Reference: 2017-167. H9 cells were dissociated using Accutase (Stem Cell Technologies, 7922) and 9000 cells were seeded in 96-well U bottom plates (Nunclon sphere, 15396123) per well. Cells were cultured in DMEM-F12 with 20% KO serum (ThermoFisher), supplemented with NEAA, penicillin/streptavidin and 100 µM β-mercaptoethanol (ThermoFisher) plus morphogens: 5 µM SB (SB431542, Sigma, S4317) and 3 µM IWR1 (Sigma, 681669) for 14 days. Rock inhibitor (Y-27632 2HC, Bio-Connect) was added until day 6 (20 µM d0-d2, 10 µM d2-d6). Organoids were cultured in DMEM-F12 medium supplemented with N2 (ThermoFisher,

17502048) and B27 (ThermoFisher, 11500446, 11530536) from day 14 and grown on orbital shakers (75 rpm) from day 21 and in bioreactor tubes (Bioké) from approximately day 46, speed 75 rpm. At day 70, 1% of matrigel (Corning, 11523550) was added to the culture. Medium was changed every 2 or 3 days.

SARS-CoV2 infection

All experiments have been conducted by the GIGA Viral platform (www.gigaviralvectors.uliege.be) in a Biosafety Level 3 lab under the environmental permit for GMO/pathogens-related activities: EDII/1/1380C38/TL/pm. For the experiments, we used the SARS-CoV2 strain (BetaCov/Belgium/GHB-03021/2020 (EPI ISL 407976|2020-02-03))[37] wild or recombinant SARS-CoV-2 strain harboring a mNeonGreen reporter.[38] VeroE6 cells were used to generate the SARS-CoV2 viral stock. The plaque assay method was used to determine the virus titer or plaque-forming unit (PFU).[32] All SARS-CoV2 infections were performed for 3 hours followed by removal of the viral particles and a media change. Samples were analyzed following 24 hours, 72 hours, or 2 weeks post-infection (long-stage post-infection).

RNA sequencing, data analysis, and differential expression analysis

High-quality RNA samples RIN values (8-10) were used for sequencing. Four samples of CTRL hCOs from 2 independent differentiations, and 4 samples from SARS-CoV2 72 hours post-infected hCOs from 2 different experiments were analyzed. The extracted RNA-seq libraries were generated by the GIGA Genomic platform (www.gigagenomics.uliege.be) using Illumina Stranded Total RNA Prep Ligation with Ribo-Zero Plus following the manufacturer protocol (Illumina ref: 20040529) and sequenced using the Illumina Novaseq 6000 sequencer, generating pair end 2 × 150bp reads. Downstream analysis was performed on R using DESeq2 method for normalization, clustering, and differential expression analysis.

Statistical analysis

All statistical analyses were performed using GraphPad (Prism). All data were first tested for normality with a Shapiro-Wilcoxon test and based on the result of this test, the parametric or corresponding non-parametric version of the test was used. The test for multiple comparisons was chosen based on the recommendation from GraphPad Prism. All information concerning the test used and the multiple comparisons test applied are found in the legend of the corresponding figure.

Results

SARS-CoV2 virus consistently infects human cortical organoids albeit at low levels

We aimed to test the infectivity and to identify the downstream effects of SARS-CoV2 viral infection in the human brain by means of an in vitro human cortical organoid model (hCO).[36,39] For this purpose, hCOs[36] of 2, 3.5 and 5-6 months in vitro (2M, 3.5M, 5-6M) were incubated for 3 hours with SARS-CoV2 viruses[37] at a 0.5 multiplicity of infection (MOI) previously reported for assessing SARS-CoV2 infectivity of brain organoids,[32] and analyzed 1 day (24 hours) or 3 days (72 hours) after infection (Figure 1A). Immunolabelings of hCOs revealed the presence of SARS-CoV2 nucleocapside (NC) proteins in less than 0.1% of hCO cells (Figure 1B-K and Supplementary Movie S1). No difference was observed between the different hCO stages analyzed for the number of cells infected (NC+), nor between different times after infection (Figure 1J). We reasoned that the exposition of hCOs to a higher viral load would result in increased cell infectivity. Our results showed that doubling the MOI of SARS-CoV2 exposure led to a higher level of infectivity of hCOs, suggesting that SARS-CoV2 infection follows a dose-dependent response (Figure 1L-M). In contrast, and as expected, a similar approach using kidney Vero cells, a susceptible cell type for SARS-CoV2 infection,[40] resulted in a higher level of infectivity at all SARS-CoV2 multiplicities of infection tested (Supplementary Figure S1). Next, we analyzed the level of expression of known SARS-CoV2 receptors and co-receptors in the hCOs. RNA sequencing of late stage (6M) hCOs confirmed low expression of the major SARS-CoV2 receptor, *ACE2*,[2,16,17] and higher expression of some of the SARS-CoV2 co-receptors such as *NRP1*, *CD147/BSG*; *GRP78/HSPA5*; *DPP4* and *AXL*[7,16,18-26] as well as some of the enzymes involved in the cleavage of the SARS-CoV2 virus spike protein to mediate viral entry to the cell, such as transmembrane serine protease 2 (*TMPRSS2*), cathepsin B (*CTSB*), cathepsin L (*CTSL*) and furin[14,23] (Figure 1N). Immunolabelings confirmed the low/absence of expression of ACE2 in mouse cortex samples and in human brain organoids (Supplementary Figure S2A). In contrast, ACE2 expression was detectable in kidney Vero cells[40] (Supplementary Figure S2B). In agreement with our RNAseq data, we could detect the expression of NRP1 in human brain organoids and in mouse cortex (Supplementary Figure S2C).

These results indicate that human cortical organoids are susceptible to infection by the SARS-CoV2 virus albeit at low levels, possibly due to the low levels of ACE2 present in the brain. Moreover, our results also suggest that some ACE2 co-receptors and proteases involved in entry of the SARS-CoV2 virus in the cells are expressed in human cortical organoids.

Deep layer projection neurons and astrocytes are the major cell types infected by SARS-CoV2 virus in hCOs at late stages in vitro

Next, we sought to analyze the cell identity of SARS-CoV2-infected cells in hCOs at different stages of maturation. First, we tested the infectivity of progenitors in hCOs from 2M up to 5-6M in vitro. Our experiments showed negligible numbers of either PAX6 or KI67 progenitor/proliferating cells infected by SARS-CoV2 in hCOs at any of the time points tested (Supplementary Figure S3A-D). Contrarily, we found that significant numbers of CTIP2+ deep layer projection neurons, and to a lesser extent CUX1+ upper layer callosal neurons were infected in hCOs at early (2M, 3.5M), and later (5-6M) time points (Figure 2A-D). Strikingly, hCOs at later stages also showed a significant number of calbindin+ (CALB+) positive interneurons[41] and GFAP+ astrocytes infected (Figure 2E-H). The overall analysis of the cell type identity among SARS-CoV2 infected cells in hCOs at 5-6M revealed that ~40% of the infected cells corresponded to GFAP+ and S100β+ astrocytes, followed by ~25% CTIP2+ cells, ~15% CALB+ cells and about ~3% CUX1+ cells (Figure 2I and Supplementary Figure S3E). Further, we investigated which percentage of cells was infected among a specific cell type population in hCOs at 5-6 months. This analysis revealed that astrocytes were the cell type showing the highest

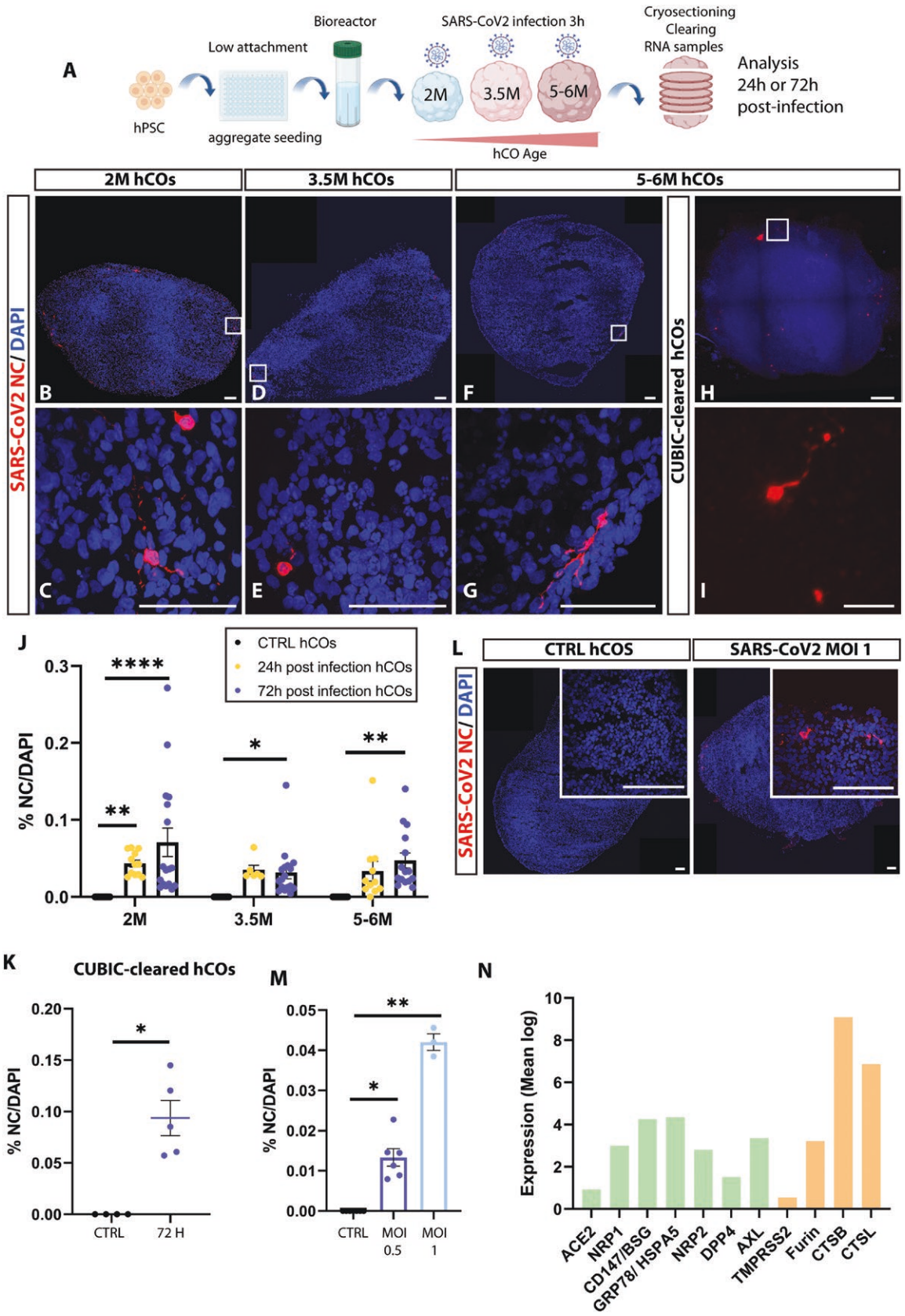

Figure 1. SARS-CoV2 infects human cortical organoids at different stages in vitro. (A) Schematic illustration of the procedure followed for derivation of human cortical organoids of different stages in vitro (2M, 3.5M, and 5-6M), hCO infection by SARS-CoV2 viral particles, and subsequent analysis. Created with BioRender.com. (B-G) Tile-Scan (B,D,F) and single (C,E,G) confocal images of cryosections immunostained for the SARS-CoV2 antigen nucleocapside (NC) in 72 hours SARS-CoV2 post-infection hCOs at all time points (2M, 3.5M, 5-6M). (H-I) Tile-Scan (H) and single (I) light-sheet microscope images of clarified (CUBIC) 72 hours SARS-CoV2 post-infected hCOs and immunostained for NC at 6M. Counterstaining was performed using DAPI. (J) Quantification of the percentage of NC+ cells among the total number of DAPI+ cells, in control (CTRL), 24 hours and 72 hours SARS-CoV2 post-infection hCOs at 2M, 3.5M, and 5-6M in vitro. Data are represented as mean percentages ± SEM (3-4 differentiations: CTRL *n* = 15-18;

24 hours $n = 6$-12; 72 hours $n = 15$-17). Two-way ANOVA with Tukey's multiple comparison test $^{*}P < .05$; $^{**}P < .01$; $^{****}P < .0001$. (K) Quantification of the percentage of NC+ cells 72 hours post-infection in whole clarified (CUBIC) 72 hours SARS-CoV2 6M hCOs. Data are represented as mean percentages ± SEM (CTRL $n = 4$; 72 hours $n = 5$). Mann-Whitney test $^{*}P < .05$. (L) Tile-Scan and single immunofluorescence confocal images of the SARS-CoV2 antigen nucleocapside (NC) in CTRL and following MOI 1 SARS-CoV2 infection in 3.5M hCOs. (M) Quantification of the percentage of NC+ cells in CTRL, MOI 0.5, and MOI 1 infected hCOs at 3.5M. Data are represented as mean percentages ± SEM (CTRL $n = 7$; MOI 0.5 $n = 6$; MOI 1 $n = 3$). Kruskal-Wallis with Dunn's multiple comparison test $^{*}P < .05$; $^{**}P < .01$. (N) Expression levels (mean log) of SARS-CoV2 receptors and co-receptors (in green), and of SARS-CoV2 viral entry-related proteases (in orange) in 6M hCOs ($n = 4$) from bulk RNAseq. Data are represented as mean ± SEM. Scale bars: 100 µm (B,D,F,L); 50 µm (C,E,G); 300 µm (H) and 40 µm (I).

percentage of cells infected among the total number of the specific cell population, when compared to excitatory and inhibitory neurons of the cortex (Figure 2J and Supplementary Figure S3F).

These results suggest that SARS-CoV2 can infect astrocytes, deep projection neurons, upper callosal neurons, and inhibitory neurons in the brain and identify astrocytes as the cell type with the highest susceptibility for infection in hCOs.

hCO cells infected with SARS-CoV2 do not undergo cell death

We asked whether SARS-CoV2 infectivity would lead to a higher rate of cell death in hCOs. To answer this question, we performed immunolabeling to detect activated cleaved-caspase 3 (CASP3) 24 hours or 72 hours post-exposure to SARS-CoV2, at different hCOs maturation stages in culture. Our analysis revealed no difference in the number of cleaved-CASP3 positive cells between infected and control hCOs (Figure 3A-B, G-H). In agreement, higher MOI of SARS-CoV2 virus did not lead to a higher rate of apoptosis when compared to control hCOs (Figure 3I). Moreover, almost no infected cells were found positive for cleaved-CASP3, further suggesting that the few apoptotic events detected were not SARS-CoV2-dependent (Figure 3J). On the contrary, and as shown before, Vero cells showed high levels of cleaved-CASP3 following SARS-CoV2 exposure[42] (Supplementary Figure S4). Next, we sought to examine cell density as a global measurement of cell death in hCOs, as shown previously.[43] Our analysis showed no change in cell density following SARS-CoV2 infection neither when using higher SARS-CoV2 viral particle load (Figure 3M-O). As we detected a preferential cell-type tropism for SARS-CoV2 virus combined with low levels of infectivity, we reasoned that certain hCO cell populations could be more affected than others, and/or that effects on cell death could be present in a localized manner specifically around SARS-CoV2 infected areas in hCOs. However, we found no increased number of neurons CTIP2+ or astrocytes vimentin+ (VIM) co-labeled with CASP3 following SARS-CoV2 infection compared to control (Figure 3C-F, K-L). In addition, we found no change in the percentage of proliferative progenitors (KI67+), deep and upper cortical layer neurons (CTIP2+, CUX1+), or interneurons (CALB+)[41] in SARS-CoV2 infected hCOs compared to control (Figure S3G-J). Next, we measured cell density and nuclei area within SARS-CoV2 infected regions (NC+) to unravel localized cell death effects in hCOs. This analysis showed no difference in local cell death, neither following higher viral particle load (Figure S5A-E), nor specifically on nuclei surrounding NC+ GFAP+ or NC + S100b+infected astrocytes (Supplementary Figure S5F-G), nor on GFAP+ or S100b+ nuclei surrounding NC+ cells (Supplemenntary Figure S5H-I).

These results overall suggest that infection by SARS-CoV2 does not trigger global, nor local, nor cell-type-dependent effects on cell death at the time points tested in hCOs.

SARS-CoV2 virus infects different brain regional identities in vitro

To test the tropism of SARS-CoV2 in the central nervous system, we infected human brain organoids with rostral and caudal regional identities. For this purpose, we generated brain organoids (BOs) with ventral telencephalic medial ganglionic eminences (MGE) identity, which are enriched in cortical interneurons and their progenitors[44-46]; BOs that model the thalamus (THL)[47]; and some that recapitulate features of the cerebellum (CRB).[48] We exposed hCOs, MGE BOs, THL BOs, and CRB BOs to SARS-CoV2 virus MOI 0.5 and measured its effects after 72 hours post-infection in vitro. Our analysis revealed that MGE BOs had the highest percentage of NC + cells compared to hCOs, THL BOs, or CRB BOs (Figure 4A-G). Next, we measured the level of apoptosis-related events in those different brain regional identity BOs by measuring the percentage of cleaved-CASP3+ cells. This analysis revealed that SARS-CoV2 infected MGE BOs, THL BOs, and CRB BOs showed no difference in the percentage of cleaved-CASP3+ cells compared to controls, similar to the previous data obtained with hCOs (Figure 4H).

These results suggest that rostral forebrain telencephalic, diencephalic, and caudal hindbrain regions of the brain show susceptibility to SARS-CoV2 infection; with MGE identities showing the highest number of cells infected in vitro.

SARS-CoV2 infection in hCOs increases the expression of pro-inflammatory, pro-survival and astrogliosis-related genes

Next, we analyzed the overall impact of SARS-CoV2 infection on cell populations in hCOs. To address this, we analyzed 5-6M infected and control hCOs by bulk RNA sequencing to unravel genes and pathways affected following infection by SARS-CoV2. First, we validated the expression of SARS-CoV2 viral genes in infected hCOs (Figure 5A). We did not detect statistical changes in the expression of SARS-CoV2 receptor and co-receptors following SARS-CoV2 infection of hCOs (Supplementary Figure S6A). Next, we analyzed genes differentially expressed between infected and control hCOs ($P_{adj} < .05$). We found that several genes related to astrocyte-mediated inflammation and astrogliosis such as alpha-1 antichymotrypsin (*SERPINA3*),[49,50] S100 calcium-binding protein A10 (*S100A10*),[51,52] homing cell adhesion molecule (*CD44*),[50,53-55] and the interleukin 13 receptor subunit alpha1 (*IL13RA1*), the immune system-related gene complement factor I (*CFI*), and the epidermal growth factor receptor (*EGFR*) were dysregulated following SARS-CoV2 infection in hCOs. In addition, the expression of lipid-metabolism-related genes, which are associated with astrogliosis,[56] such as phospholipase C-delta-3 (*PLCD3*) and phospholipase C-delta-1 (*PLCD1*) were also affected in infected hCOs. Interestingly, instead of effects promoting cell death pathways, we detected an upregulation of the cell survival-related genes, such as

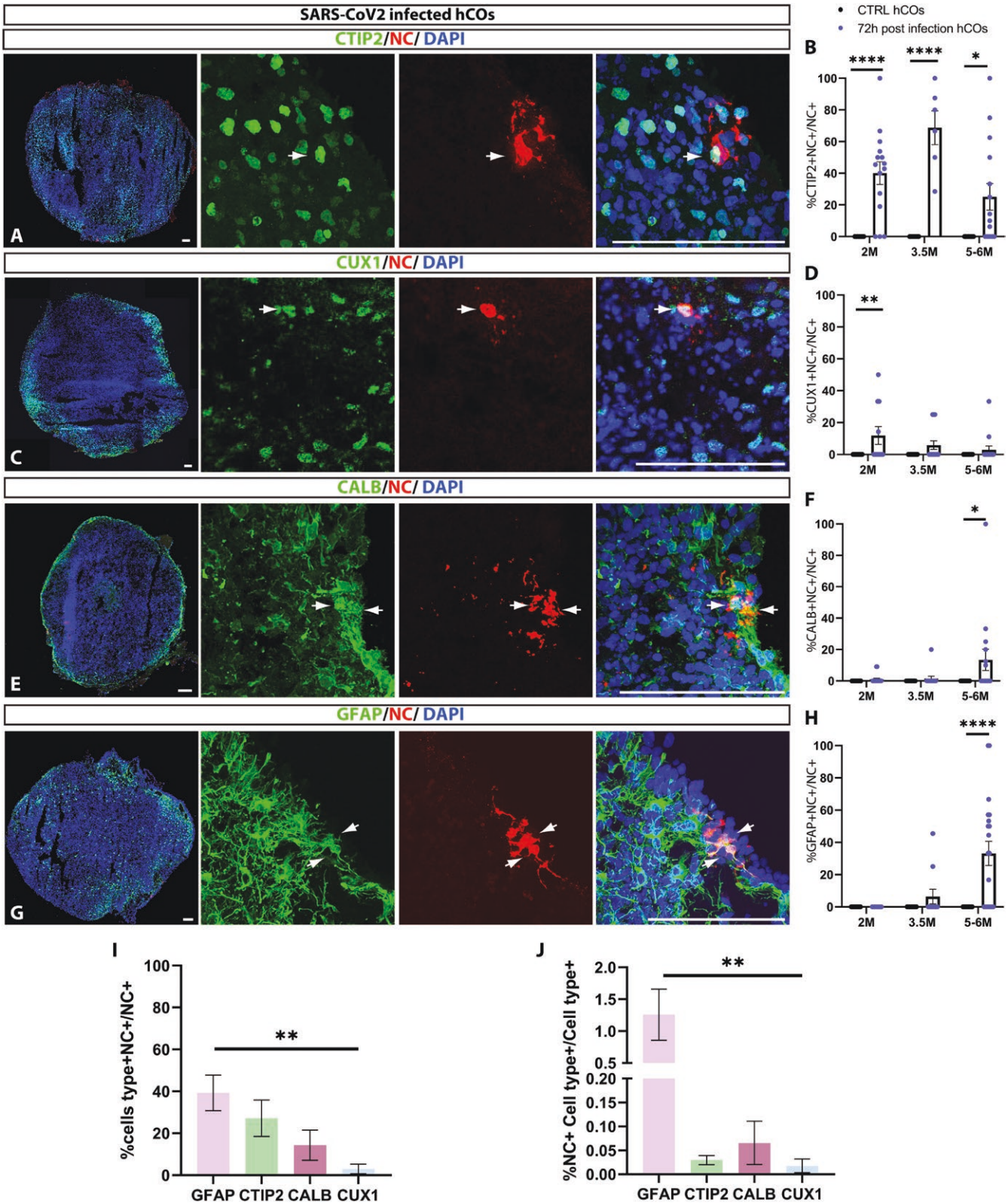

Figure 2. SARS-CoV2 infects mostly astrocytes at late stages in hCOs. (A,C,E,G) Tile-Scan (left panel) and single confocal images of cryosections immunostained for the SARS-CoV2 antigen nucleocapside (NC) and the deep layer cortical neuronal marker CTIP2 (A); the upper layer cortical neuronal marker CUX1 (C); the interneuron marker calbindin (E), or the astrocyte marker GFAP (G) in 6M 72h post-infection hCOs, and high magnification insets. Counterstaining was performed using DAPI. (B,D,F,H) Quantification of the percentage of double-positive CTIP2 + NC + (B); CUX1 + NC + (D); CALB + NC + (F); GFAP + NC + (H), among the total NC + population in 2M, 3.5M, and 5-6M 72h post-infected SARS-CoV2 hCOs compared to control (CTRL). Data are represented as mean percentages ± SEM (2-3 differentiations: CTRL n = 8-20; 72 hours n = 11-20). Two-way ANOVA with Tukey's multiple comparison test $^{*}P < .05$; $^{**}P < .01$; $^{****}P < .0001$. (I) Percentage of specific cell types double positive for NC among the total NC+ population in 5-6M 72 hours post-infected SARS-CoV2 hCOs. Data are represented as mean percentages ± SEM (3-4 differentiations: 72 hours n = 14-16). Two-way ANOVA with Tukey's multiple comparison test $^{**}P < .01$. (J) Percentage of NC + infected cell type among the total number of the cell type-specific population in 5-6M 72 hours post-infected SARS-CoV2 hCOs. Data are represented as mean percentages ± SEM (3-4 differentiations: 72 hours n = 15-20. Two-way ANOVA with Tukey's multiple comparison test $^{*}P < .05$; $^{**}P < .01$. Scale bars: 100 µm (A,C,E,G). White arrows show cells double positive for NC and the specific cell-type marker tested (A,C,E,G).

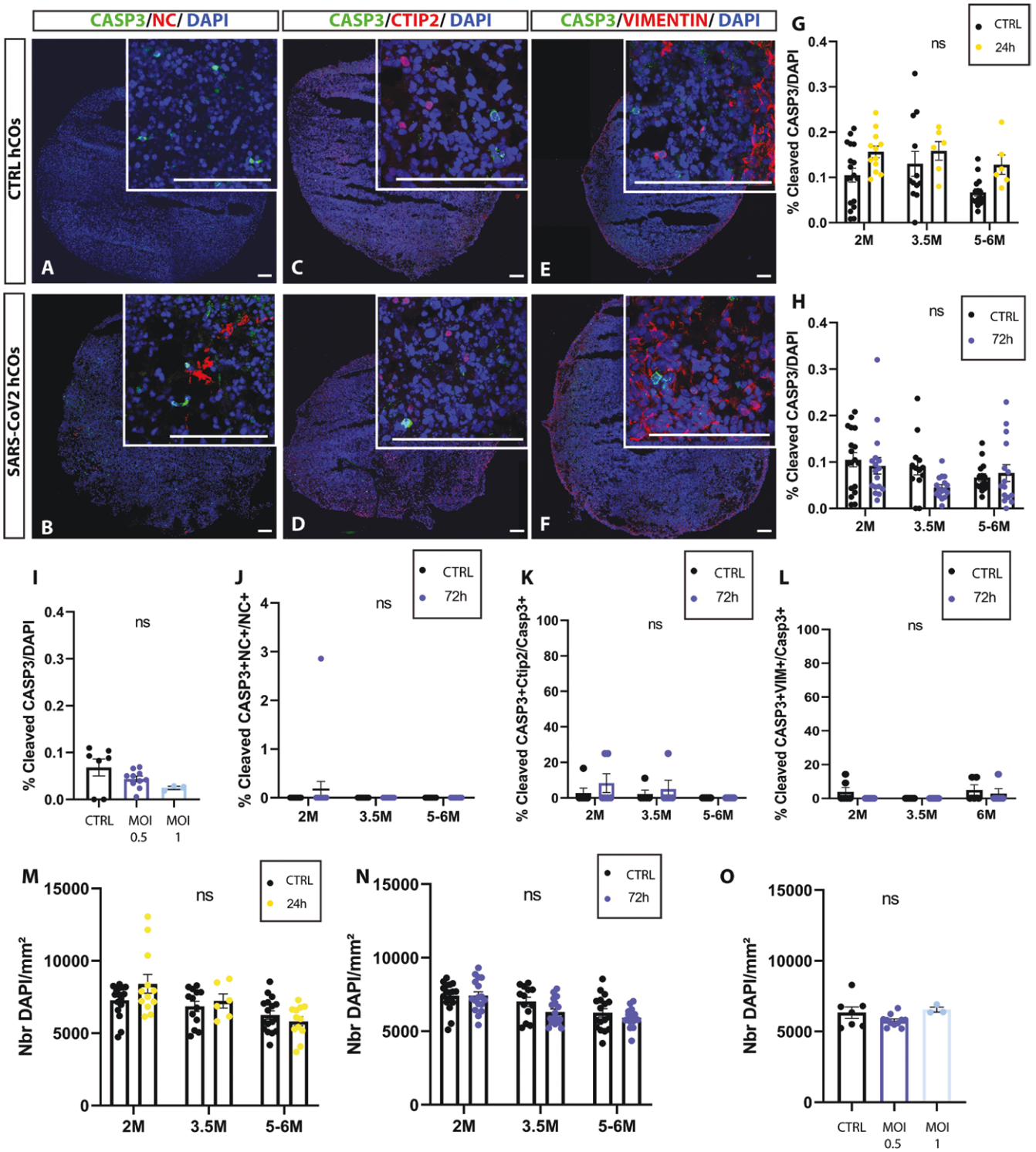

Figure 3. SARS-CoV2 infectivity does not induce cell death in hCOs. (A-F) Tile-Scan and single confocal images of cryosections immunostained for the apoptotic marker caspase 3 (CASP3) + cells and either the SARS-CoV2 antigen NC; the cortical layer V marker CTIP2; or the astrocyte marker VIM in 5-6M CTRL and 72 hours post-infected hCOs and high magnification pics (insets). Counterstaining was done with DAPI. (G-I) Quantification of the percentage of CASP3 + cells among the total number of cells DAPI + in CTRL and 24 hours post-infected hCOs (G), in CTRL and 72 hours post-infected hCOs (H), or in CTRL, MOI 0.5 and MOI 1 (I) infected hCOs. Data are represented as mean percentages ± SEM (1-3 differentiations: 2M n = 12-18; 3.5M n = 3-16; 5-6M n = 6-15). Two-way ANOVA with Sidak's multiple comparison test (G-H) and one way ANOVA with Tukey's multiple comparison test (I). (J) Quantification of the percentage of double positive cells CASP3 + NC+ among the NC + population. Data are represented as mean percentages ± SEM (3 differentiations: 2M n = 17-18; 3.5M n = 13-16; 5-6M n = 15). Two-way ANOVA with Tukey's multiple comparison test, ns: non-significant. (K-L) Quantification of the percentage of double positive cells CASP3 + CTIP2 + among CASP3 (K), and CASP3 + VIM + among CASP3 + (L) at all stages. Data are represented as mean percentages ± SEM (1 differentiation: 2M n = 6; 3.5M n = 5; 5-6M n = 5). (G-K) Two-way ANOVA with Sidak's multiple comparison test, ns = non-significant. (M-O) Quantification of the cell density (number of DAPI cells per mm²) in CTRL and 24 hours (M), CTRL and 72 hours (N), or in CTRL, MOI 0.5 and MOI 1 infected hCOs (O). (M-N) Data are represented as mean percentages ± SEM (3 differentiations: 2M n = 12-17; 3.5M n = 6-17; 5-6M n = 12-17). Two-way ANOVA with Sidak's multiple comparison test. ns: non-significant. (O) Data are represented as mean percentages ± SEM (1 differentiation: CTRL n = 7; MOI 0.5 n = 6; MOI 1 n = 3). One-way ANOVA test with Tukey's multiple comparison test ns: non-significant. Scale bars: 100µm (A-F).

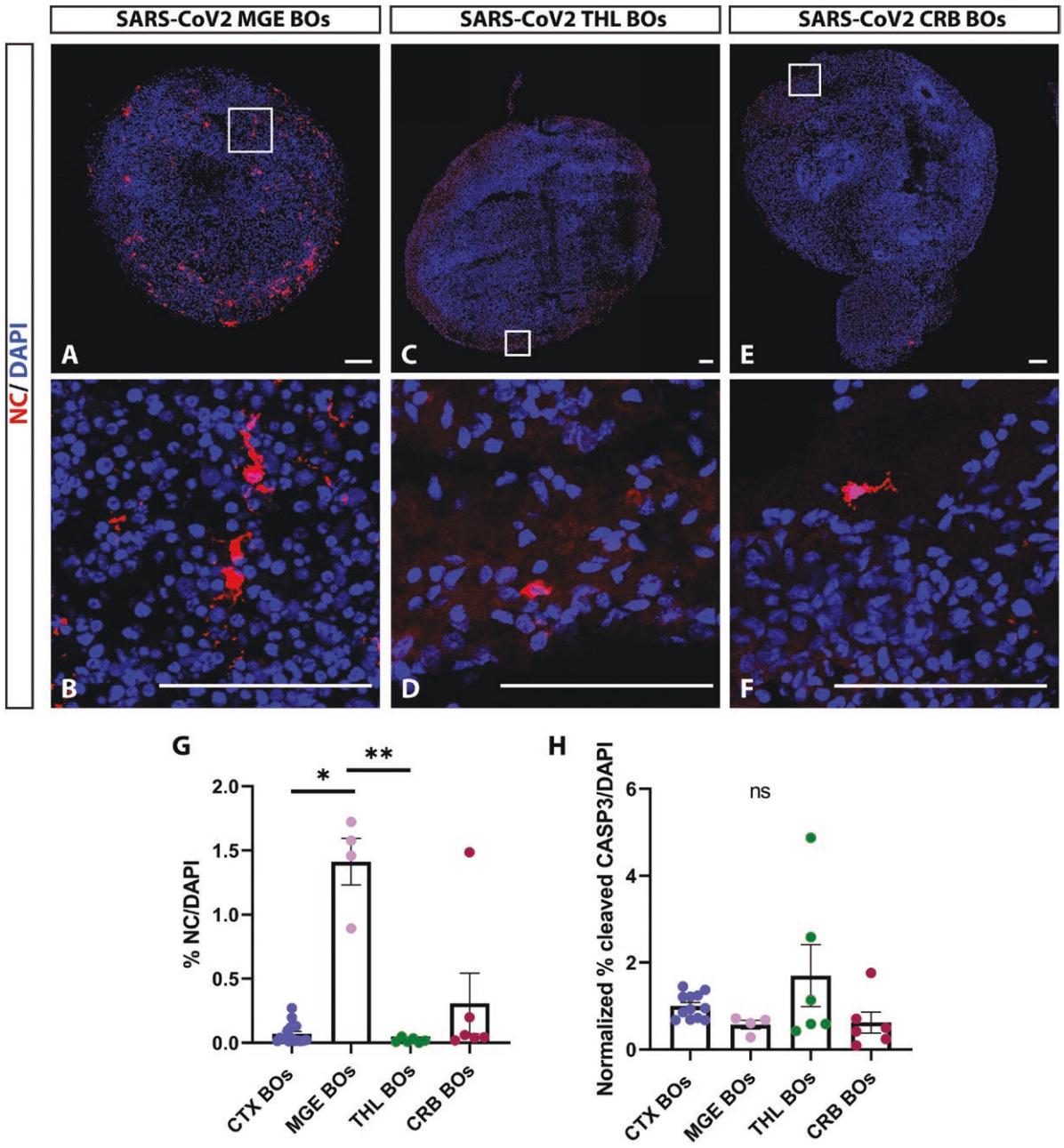

Figure 4. SARS-CoV2 virus infects different brain regional identity BOs in vitro. (A-F) Tile-Scan (A,C,E) and single (B,D,F) confocal images of cryosections immunostained for the SARS-CoV2 antigen nucleocapside (NC) in 72h MGE BOs (A-B), THL BOs (C-D), and CRB BOs (E-F) at 2M. Counterstaining was performed using DAPI. (G) Quantification of the percentage of NC + cells among the total number of cells DAPI+ in CTX hCOs, MGE BOs, CRB Bos, and THL BOs. Data are represented as mean percentages ± SEM (CTX $n = 17$; MGE $n = 4$; CRB $n = 6$; THL $n = 6$). Kruskal-Wallis test with Dunn's multiple comparison test. $^{*}P < .05$; $^{**}P < .01$. (H) Quantification of the relative percentage of CASP3+ cells among the total number of cells DAPI+ in SARS-CoV2 infected CTX hCOs, MGE BOs, CRB Bos, and THL BOs compared to CTRL CTX hCOs, MGE BOs, CRB Bos, and THL BOs expressed as 1. Data are represented as normalized mean percentage ± SEM (CTX $n = 17$; MGE $n = 4$; CRB $n = 6$; THL $n = 6$). Kruskal-Wallis test with Dunn's multiple comparison test. Data were normalized by the mean value of control hCOs samples, ns: non-significant. Scale bars: 100μm (A-F).

superoxide dismutase 2 (*SOD2*),[57] brain and acute leukemia cytoplasmic protein (*BAALC*),[58,59] and the cytokine hepatocyte growth factor (*HGF*)[60] following SARS-CoV2 infection (Figure 5B-C and Supplementary Table S1). Top candidate pathways (enrichR) and gene set enrichment analysis (GSEA) revealed the link of oxidative phosphorylation, glycolysis, TNFA signaling via NFKB, protein secretion, inflammatory responses, epithelial-mesenchymal transition, and lipid metabolism-related pathways (Figure 5D-E, Supplementary Figure S6B and Supplementary Tables S2 and S3). Interestingly, the expression of genes related to glycolysis and lipid metabolism, as well as the epithelial-mesenchymal transition pathway have been shown to be correlated with astrogliosis.[56,61]

Next, we analyzed the impact of SARS-CoV2 infectivity on the astrocyte population since they are the most frequent cell type infected in hCOs. Our results showed that SARS-CoV2 infected hCOs had a lower GFAP+ organoid area coverage as compared to controls (Figure 5F-I, L). While this phenotype did not result from the reduction in number of astrocytes in infected hCOs (Figure 5M), our analysis revealed that SARS-CoV2 infected astrocytes had a reduced area as compared to control astrocytes (Figure 5J-K, N).

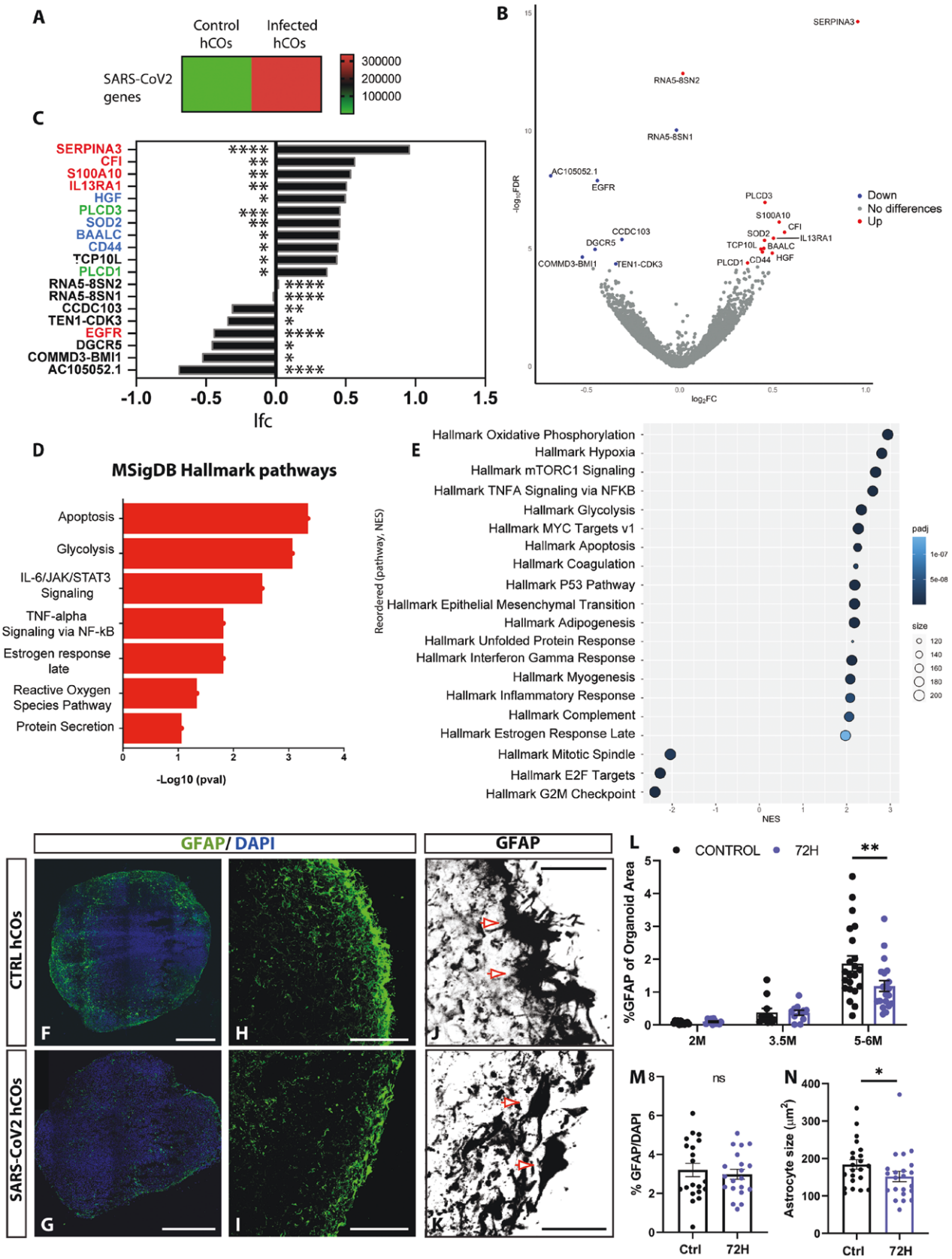

Figure 5. SARS-CoV2 infection leads to astrocyte morphological changes and overall pro-inflammatory transcriptomic changes in hCOs. (A) Heatmap representation of SARS-CoV2 normalized counts in CTRL or 72 hours SARS-CoV2 post-infected 5-6M hCOs. (B) Volcano plot representation of the changes in genes expression (DEG) in 5-6M 72h SARS-CoV2 post-infection hCOs compared to CTRL hCOs, representing the Log2foldChange (log_2FC) and the P_{adj} value ($-log_{10}FDR$). Genes with a P_{adj} value below 0.05 and with a negative Log2foldChange are represented in blue (downregulated genes), and genes with a P_{adj} value below.05 with a positive Log2foldChange are represented in red (upregulated). Genes that have a P_{adj} value above.05 are represented in grey (non-significantly changed). (C) Bar graph representation of the log fold change (lfc) of the differentially expressed genes in 72 hours

post-infected hCOs compared to CTRL hCOs. In red: Astrocyte-mediated inflammatory genes; in green: lipid metabolism-related genes; in blue: cell survival-related genes. (D) Representation of the top pathways from MSigDB Hallmark pathways database based on the significance of enrichment of upregulated and downregulated DEGs. (E) Bubble plot of the Gene Set Enrichment Analysis (GSEA) representing the enriched pathways with a P_{adj} value < .0001. Pathways that have a normalized enrichment score (NES) positive > 0 are upregulated whereas pathways with a NES negative < 0 are downregulated. Pathways were ordered by the NES score in a decreasing manner. Size represented the number of genes from the RNAseq presented in the pathway. All data were generated from bulk RNAseq analysis of 2 independent differentiations (CTRL $n = 4$; 72 hours $n = 4$). $^{*}P < .05$; $^{**}P < .01$; $^{***}P < .001$; $^{****}P < .0001$. (F-K) Tile-Scan (F-I) and single (J-K) confocal images of cryosections immunostained for the astrocyte marker GFAP (F-K) in 5-6M CTRL and 72 hours post-infected hCOs. Counterstaining was performed using DAPI. (L) Percentage of organoid area covered by GFAP+ cells in CTRL and 72 hours hCOs of 2M, 3.5M, and 5-6M. Data are represented as mean percentages ± SEM (2-4 differentiations: 2M $n = 6$-12; 3.5M $n = 6$-11; 5-6M $n = 12$-22). Two-way ANOVA with Sidak's multiple comparison test $^{**}P < .01$. (M) Quantification of the percentage of GFAP+ cells among the total number of cells DAPI+ in CTRL and 72 hours post-infected 5-6M hCOs. Data are represented as mean percentages ± SEM (4 differentiations: CTRL $n = 23$; 72 hours $n = 20$). Mann-Whitney two-tailed test $^{*}P < .05$. (N) Quantification of astrocyte area in CTRL and 72 hours post-infected 5-6M hCOs. Data are represented as mean percentages ± SEM, (4 differentiations: CTRL $n = 22$ organoids; 72 hours $n = 22$ organoids). Mann-Whitney two-tailed test $^{*}p < .05$. Scale bars 500 µm (F-G); 100 µm (H-I); 25 µm (J-K). Red arrows show examples of representative astrocytes (E,F).

Next, we further analyzed the expression of candidate pro-inflammatory *SERPINA3* and pro-survival *SOD2* genes in infected hCOs, as they could have important implications in the inflammatory cascades following SARS-CoV2 infection in hCOs. Our analysis revealed higher expression of the astrogliosis marker SERPINA3 and the pro-survival gene SOD2 in hCOs 72 hours post-infection compared to control (Figure 6A-F, M). Moreover, we specifically found a higher percentage of astrocytes expressing SOD2 in hCOs 72 hours post-infection compared to control astrocytes, suggesting that astrocytes in infected hCOs switch on the expression of the *SOD2* gene as a mechanism against viral infection to promote anti-apoptotic pathways (Figure 6G-I). In line with this observation, we found a lower percentage of cells labeled for gamma H2AX, a marker of DNA damage in the cell (Figure 6J-L). Finally, we investigated the cellular effects triggered by SARS-CoV2 in hCOs 2 weeks long-stage (2W LS) post-infection (Figure 7A). Two weeks LS hCOs had a trend for higher total number of NC+ cells (Figure 7B-C, H) and increased number of GFAP + NC + and CTIP2 + NC+, however, no change in percentage of CTIP2+, nor GFAP+ infected cells among total NC+ cells was detected (Figure 7B-C, I-J and Supplementary Figure S7A-B) when compared to 72 hours. These data suggest no change in cell type tropism but an overall higher number of infected cells. No difference in cell death mechanisms such as CASP3+ cells for apoptosis (Supplementary Figure S7C-H, I-L), pMLKL+ cells for necroptosis[62] (Supplementary Figure S7M), nor difference in global or local cell density was detected in 2W LS hCOs compared to control or 72h (Supplementary Figure S7 N-P). In agreement with our previous results, we observed a reduction of GFAP+ hCO area in 2W LS (Figure 7B-C, K). Remarkably, increased expression of CD44 and S100A10 was detected within the astrocyte population in 2W LS hCOs (Figrue 7D-G, L-N).

Overall, these results suggest that SARS-CoV2 infection triggers astrocyte morphological changes and increased expression of *SERPINA3*, *CD44,* and *S100A10* astrogliosis-related genes. Moreover, SARS-CoV2 infection causes an overall increased expression of pro-inflammatory genes and upregulation of pro-survival pathways that may counteract cell death mechanisms thereby promoting resilience of dysregulated cells in hCOs.

Discussion

The understanding of the ability of the SARS-CoV2 virus to infect the human brain has so far remained elusive due to the fact that only a few studies have reported the presence of viral RNA in CSF from COVID-19 patients or detected the presence of the virus in postmortem brain samples.[9,30,63,64] However, neurological manifestations are present in about at least a third of COVID-19 patients suggesting the possibility that pathological effects are triggered in the brain of patients.[65] Lack of SARS-CoV2 particle detection in the brain may result from the challenge of accessing CSF and/or brain tissue from COVID-19 patients during critical phases of SARS-CoV2 infection, possibly combined with a low level of infectivity of SARS-CoV2 in the brain when compared to other tissues such as the respiratory system. In support of this hypothesis, a recent study based on 11 autopsies from COVID-19 patients at different stages of the disease and using novel technologies for RNA detection (droplet digital PCR) succeeded in showing the presence of SARS-CoV2 RNA in 10 out of 11 of the brain samples analysed.[10] However, a limitation of this and similar previous studies is that patient cohorts may have been more susceptible for SARS-CoV2 infectivity and its pathological downstream effects than control groups, due to preexistent unrelated medical conditions that finally led to their death from severe COVID-19. Moreover, previous concerns are the contamination of brain samples with blood cells or lung tissue during the autopsy procedure that could lead to false positive detection of SARS-CoV2. The aim of the current study is to analyze the ability of SARS-CoV2 to infect the brain, to distinguish its tropism towards different brain cell types, and to unravel major downstream effects of SARS-CoV2 infection in brain using a long-term human in vitro cortical organoid model.

The infectivity of SARS-CoV2 has been previously assessed in human telencephalic organoids derived from default differentiation paradigms and compared to that in choroid plexus organoids. This study found mostly infectivity of SARS-CoV2 restricted to choroid plexus cells with the absence or minimum detection of virus RNA or protein in other brain organoid cell types.[32] Later reports using different brain organoid models reported however infectivity of the virus in brain cells besides choroid plexus cells.[33,66-70] Most of these studies reported a similar infectivity rate among cell types, including progenitors, neurons, and glia cells, or on the contrary, higher infectivity in neurons.[33,66-68,70,71] Some recent studies have suggested a specific cellular tropism of SARS-CoV2 for astrocytes in the brain.[19,35] However, a systematic and quantitative analysis of brain cell types susceptible to SARS-CoV2 infection in brain organoids and the analysis of different brain organoid maturation stages in vitro including long-term cultures has not yet been performed. Here we present an exhaustive analysis of regionalized brain organoids at 3 different in vitro stages

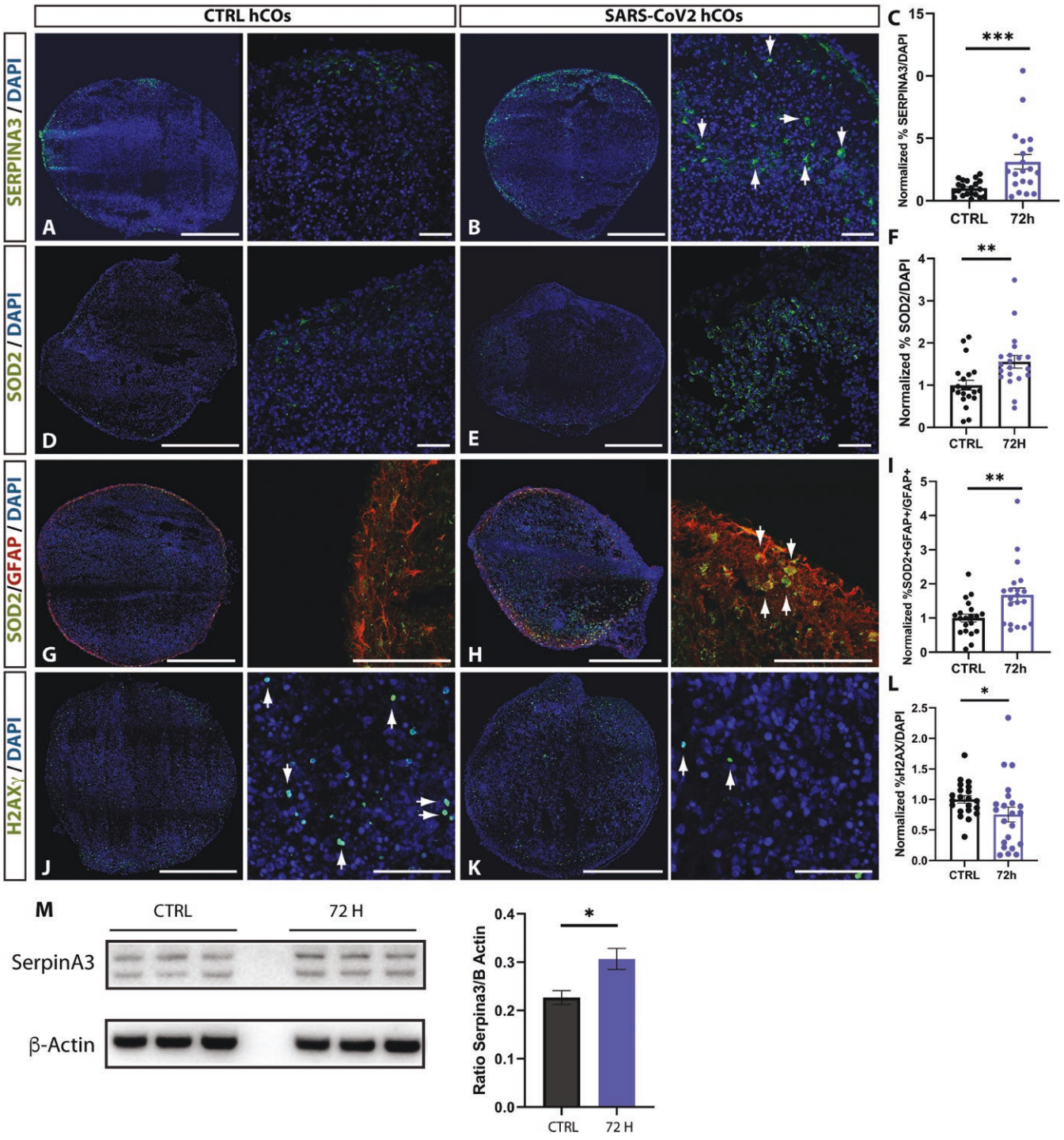

Figure 6. Increased expression of astrogliosis-related markers and pro-survival genes in infected hCOs. (A-B,D-E,G-H,J-K) Tile-Scan and single confocal images of cryosections immunostained for the astrogliosis marker SERPINA3 (A-B), the pro-survival gene SOD2 (D-E, G-H), the astrocyte marker GFAP (G-H), and the DNA double-strand break marker gamma H2AX (J-K) in 5-6M CTRL and 72 hours post-infected hCOs. Counterstaining was performed using DAPI. White arrows show cells double positive for SOD2 and GFAP (H). (C,F,I,L) Quantifications of the percentage of SERPINA3+ (C), SOD2+ (F), SOD2+GFAP + (I) and gamma H2AX+ (L) cells over the total number of DAPI+ in control and 72 hours post-infected 5-6M hCOs. Data are represented as mean percentages ± SEM (4 differentiations: CTRL $n = 20$; 72 hours $n = 20$). (C,F) Mann-Whitney test $^{**}P < .01$; $^{***}P < .001$ (I) Mann-Whitney test $^{**}P < .01$. (L) Two-tailed *t*-test $^{*}P < .05$. (M) Western blot detection of SERPINA3 and β-actin levels from protein extracts of CTRL and 72 hours infected hCOs. MW for SERPINA3 is approximately. 52 and 60 kDa. Quantification of the levels of SERPINA3 in CTRL and 72 hours post-infected hCOs normalized with β-actin levels. Data are represented as mean value ± SEM (2 differentiations, 3 replicates ($n = 8$ organoids/sample). *T*-test $^{*}P < .05$. Data were normalized by the mean value of control hCOs samples. Scale bars: 500 µm (A-K) and 50 µm (higher magnification views on the right).

up to 6 months in culture exposed to SARS-CoV2 virus that reveals consistent infectivity of the virus at all stages albeit low levels (around 0.1%). This low percentage of infectivity in cortical organoids was consistent with the low level of detection of *ACE2* at the mRNA level. Nevertheless, we could detect higher expression of some of the ACE2 co-receptors

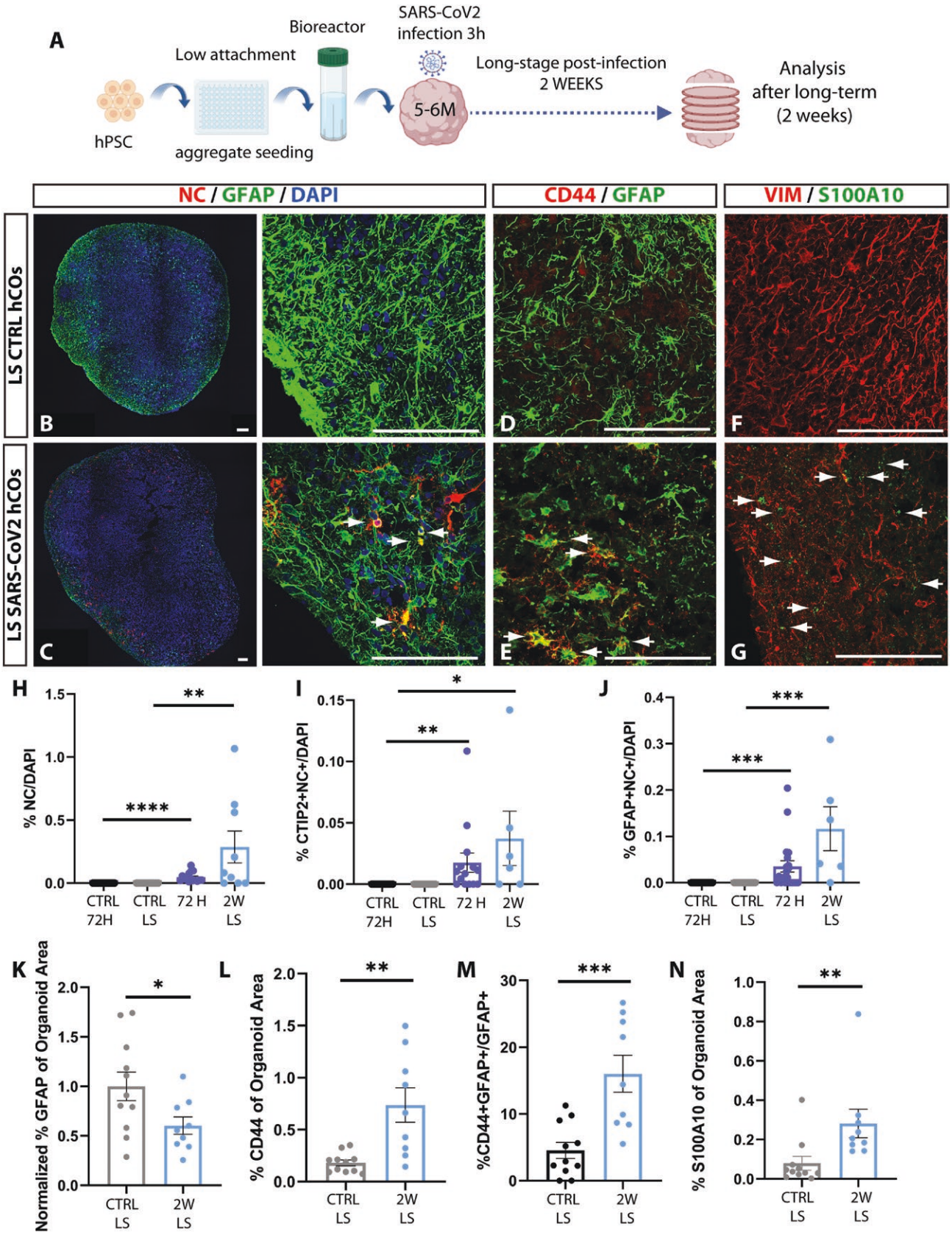

Figure 7. Long-stage post-infected hCOs show changes in GFAP hCO coverage and upregulation of CD44 and S100A10 astrogliosis markers. (A) Schematic illustration of the procedure followed for hCO infection by SARS-CoV2 and analysis after long-stage post-infection (2 weeks). Created with BioRender.com. (B-G) Tile-Scan (B-C) and single (D-G) confocal images of cryosections immunostained for the SARS-CoV2 antigen nucleocapside (NC; B-C) and GFAP (B-E), CD44 (D-E), VIM (F-G) and S100A10 (F-G) in LS SARS-CoV2 post-infected hCOs of 6M. Counterstaining was performed using DAPI. (H-J) Quantification of the percentage of NC + cells (H), the percentage of NC + CTIP2+ (I) or NC + GFAP+ (J), among the total number of DAPI+ in control 72 hours (CTRL 72 hours), control LS (CTRL LS), 72 hours SARS-CoV2 post-infected (72 hours) and LS 2weeks post-infected (2W LS) hCOs at 6M in vitro. Data are represented as mean percentages ± SEM (2-4 differentiations: CTRL 72 hours $n = 15$; CTRL LS $n = 11$; 72 hours $n = 15$; 2W LS $n = 9$). Kruskal-Wallis with Dunn's multiple comparison test $^{*}P < .05$; $^{**}P < .01$; $^{****}P < .0001$. (K-L, N) Quantification of GFAP + area (K), the

CD44 + area (L), and the S100A10 + area (N) in CTRL LS and 2W LS 6M hCOs. Data are represented as mean percentages ± SEM. (2 differentiations: CTRL LS $n = 11$; 2W LS $n = 9$). *T*-test (K-L), Mann-Whitney two-tailed test (*M*) $^{*}P < .05$; $^{**}P < .01$. (M) Quantification of CD44 + GFAP + cells in CTRL LS and 2W LS 6M hCOs. Data are represented as mean percentages ± SEM. (2 differentiations: CTRL LS $n = 11$; 2W LS $n = 9$). Mann-Whitney two-tailed test $^{***}P < .001$. Data were normalized by the mean value of control hCOs samples. Scale bars: 100 µm.

such as NRP1 and DPP4 and some of the proteases involved in viral entry to the cell. In contrast with previous reports, we have not found infectivity of progenitors or proliferative cells in hCOs at any of the maturation stages analyzed. Our analysis revealed a time-dependent pattern of tropism of the virus where at early stages deep projection neurons and upper callosal neurons were the most infected cell types whereas at late time points there was a switch toward astrocytes as the main target of the SARS-CoV2 virus. While the percentage of SARS-CoV2 infected cells represented around 0.1% of all hCO cells, SARS-CoV2 infected more than a 1% of the total astrocyte population at late stages in vitro, and this percentage was far higher than the one reported for any other infected cell type, suggesting a cell-type specific tropism of SARS-CoV2 for astrocytes.

In this study, we have compared the efficiency of SARS-CoV2 to infect brain organoid models that mimic different regions of the forebrain and the developing cerebellum. Intriguingly, we found that ventral telencephalic organoids (MGE) were more susceptible to SARS-CoV2 infection as compared to other regionalized organoids. Other reports have previously interrogated the infectivity of SARS-CoV2 using multiple brain organoid regionalities in vitro, however, these studies did not reveal any difference in the percentage of infectivity between organoid models.[33] Our findings suggest that cortical interneurons and/or their progenitors could be important targets of SARS-CoV2 infection. Further work is needed to assess whether cortical interneurons that are traveling towards the cortex are also susceptible to SARS-CoV2 infection and whether this would affect their migration in forebrain assembloids.[44-46]

The study of the downstream consequences of SARS-CoV2 infection in the brain has been the focus of several works for instance those reporting MRI scans-based brain abnormalities such as lesions in the white matter in COVID-19 patients 6 months post-infection.[27] However, the extent of those brain anatomical alterations did not correlate with the neurological symptoms of the patients and there was an age mismatch between the control and infected group that could lead to the anatomical differences detected. Conversely, recent studies have found no major cytopathological effect outside the respiratory tract in postmortem patient samples.[10] Previous in vitro and in vivo studies have shown an increased cell death rate among SARS-CoV2 infected cells in the brain.[9,19,35,72] However, these results are in contrast with other reports showing no major cell loss in different models.[71,73] We also aimed to clarify SARS-CoV2 downstream effects using cortical brain organoids at different stages in vitro. Our in-depth analysis showed no major effect on cell death, no change in apoptotic cell number, and no global, local, or cell-type dependent change in cell density, or nuclei size in infected cortical organoids. Our RNAseq data from infected hCOs revealed overall increased expression of inflammatory and astrogliosis-related genes[50,53-55] such as *SERPINA3*, *CD44*, *S100A10*, increased oxidative phosphorylation, TNFA signaling, and metabolic changes, which suggests broad inflammatory-induced conditions in hCOs. Interestingly, we confirmed the upregulation of the astrogliosis markers SERPINA3, CD44, and S100A10 at the protein level in infected hCOs, suggesting that SARS-CoV2 infection may lead to astrogliosis in hCOs. Surprisingly, instead of cell death mechanism activation, we detected upregulation of SOD2-related cell survival pathways, which suggests that compensatory pro-survival mechanisms are triggered in astrocytes and neuronal populations following SARS-CoV2 infection of hCOs. In agreement with this, we detected lower levels of DNA damage marked by H2AX gamma in hCOs infected by the virus, indicating possibly more efficient repair mechanisms for double-strand DNA break. These results could imply the appearance of resilient dysregulated astrocytes and neurons within an inflammatory context following SARS-CoV2 infection.

Our current study comprises 2 short-term time points after SARS-CoV2 exposure of 1 and 3 days, and an additional long-stage (2 weeks) time post-infection to understand the immediate and late major cellular and transcriptomic changes occurring in brain cell types as a direct cause of the infection of the virus. Recent studies have attempted to decipher the pathological events in COVID-19 patients suffering from SARS-CoV2-related symptoms beyond 3 months after exposure to the virus, which is known today as long-COVID.[74] It would be thus interesting in future studies to assess even longer-term effects in brain cell types following SARS-CoV2 infection in cortical organoid models.

Interestingly, some reports have hypothesized that SARS-CoV2-mediated effects in brain mimic the inflammatory conditions identified in the brains of patients suffering from neurodegenerative conditions.[19,28,73] Despite the limitation of our hCO model which lack major immune cell types, our results go in line with this hypothesis with pro-inflammatory changes triggered in our system only 1-3 days after infection of the virus combined with the activation of pro-survival pathways which could lead to survival of affected neurons and astrocytes. Strikingly, a known pro-inflammatory protein expressed in astrocytes, SERPINA3, which has been detected in plasma of middle-aged adults with high risk for dementia,[75] was also upregulated in our infected cortical organoids. One could envision cortical brain organoids infected with SARS-CoV2 as an interesting model to study susceptibility to develop dementia-like features after long-term culture that could parallel the in vivo situation of neurodegenerative patients.

Lastly, we want to remark that we cannot exclude the occurrence of cell death events following longer SARS-CoV2 post-infection time points in hCOs. Besides, our model recapitulates the presence of human neurons and astrocytes but lacks the presence of microglia cells, which could have an important role in mediating cell death mechanisms following infection. Our current analysis used a restricted number of markers to identify specific cell populations, such as astrocytes, (GFAP+, S100b + and VIM+), and few markers of astrogliosis to characterize the astrocyte response to the virus. Indeed, future studies using single-cell technologies may unravel the full pattern of transcriptomic changes within astrocyte subpopulations following SARS-CoV2 infection.

In conclusion, we show here that hCOs at 3 different maturation stages in vitro up to 6 months present a reproducible level of low infectivity following SARS-CoV2 exposure. We demonstrate that astrocytes are the most representative cell type infected, and that this ultimately leads to increased astrogliosis-related gene expression, pro-inflammatory and cell survival-related changes in the overall brain cell type populations in cortical organoids. These data unravel important pathways triggered in the brain following SARS-CoV2 infection that could be relevant for the design of future therapies aiming at protecting the brain from inflammatory dementia-like related pathological changes.

Conclusion

SARS-CoV2 infection leads to neurological symptoms in a subset of patients. Our study shows that SARS-CoV2 infects astrocytes, deep layer projection neurons, upper callosal neurons, and interneurons of the cortex and triggers astrogliosis-related gene expression, overall inflammation, and cell survival pathways.

These findings could imply the emergence of resilient dysregulated neurons and astrocytes in the context of an inflammatory environment. Our model could be instrumental in the design of future strategies aiming at lowering SARS-CoV2-related neurological effects.

Acknowledgments

We thank the GIGA lentiviral Vectors, GIGA Imaging, and GIGA Genomics and Bioinformatics platforms for their contribution, help and support to this work.

Author contributions

Ira Espuny-Camacho (Conception and design). Jean-Claude Twizere and Emmanuel Di Valentin (Resources, Investigation). Mathilde Colinet, Ira Espuny-Camacho, Ioana Chiver, Antonela Bonafina, Gérald Masset, and Daniel Almansa (Collection and/or assembly of data, Investigation). Ira Espuny-Camacho, Mathilde Colinet, Ioana Chiver (Data analysis and interpretation). Ira Espuny-Camacho (Writing—original draft). Ira Espuny-Camacho, Laurent Nguyen, Mathilde Colinet, Ioana Chiver (Writing—review & editing). Ira Espuny-Camacho and Laurent Nguyen (Final approval of manuscript).

Funding

This work was supported by the F.R.S.-FNRS #CUR 40002797 (to L. N. and I. E.-C.), and the F.R.S.-FNRS #PER 40003579 (to L. N., I. E.-C., E. dV., J-C. T.).

Conflicts of interest

The authors declare no competing interests.

Data availability

RNA sequencing data associated with this manuscript has been submitted to GEO with a submission ID: GSE250289.

Supplementary material

Supplementary material is available at *Stem Cells* online.

References

1. Zhu N, Zhang D, Wang W, et al; China Novel Coronavirus Investigating and Research Team. A novel coronavirus from patients with pneumonia in China, 2019. *N Engl J Med*. 2020;382:727-733. https://doi.org/10.1056/NEJMoa2001017
2. Kuba K, Imai Y, Rao S, et al. A crucial role of angiotensin converting enzyme 2 (ACE2) in SARS coronavirus-induced lung injury. *Nat Med*. 2005;11:875-879. https://doi.org/10.1038/nm1267
3. Ding Y, He L, Zhang Q, et al. Organ distribution of severe acute respiratory syndrome (SARS) associated coronavirus (SARS-CoV) in SARS patients: implications for pathogenesis and virus transmission pathways. *J Pathol*. 2004;203:622-630. https://doi.org/10.1002/path.1560
4. Puelles VG, Lütgehetmann M, Lindenmeyer MT, et al. Multiorgan and renal tropism of SARS-CoV-2. *N Engl J Med*. 2020;383:590-592. https://doi.org/10.1056/NEJMc2011400
5. Mao L, Jin H, Wang M, et al. Neurologic manifestations of hospitalized patients with Coronavirus Disease 2019 in Wuhan, China. *JAMA Neurol*. 2020;77:683-690. https://doi.org/10.1001/jamaneurol.2020.1127
6. Helms J, Kremer S, Merdji H, et al. Neurologic features in severe SARS-CoV-2 infection. *N Engl J Med*. 2020;382:2268-2270. https://doi.org/10.1056/NEJMc2008597
7. Varatharaj A, Thomas N, Ellul MA, et al; CoroNerve Study Group. Neurological and neuropsychiatric complications of COVID-19 in 153 patients: a UK-wide surveillance study. *Lancet Psychiat*. 2020;7:875-882. https://doi.org/10.1016/S2215-0366(20)30287-X
8. Solomon IH, Normandin E, Bhattacharyya S, et al. Neuropathological features of Covid-19. *N Engl J Med*. 2020;383:989-992. https://doi.org/10.1056/NEJMc2019373
9. Crunfli F, Carregari VC, Veras FP, et al. Morphological, cellular, and molecular basis of brain infection in COVID-19 patients. *Proc Natl Acad Sci U S A*. 2022;119:e2200960119. https://doi.org/10.1073/pnas.2200960119
10. Stein SR, Ramelli SC, Grazioli A, et al; NIH COVID-19 Autopsy Consortium. SARS-CoV-2 infection and persistence in the human body and brain at autopsy. *Nature*. 2022;612:758-763. https://doi.org/10.1038/s41586-022-05542-y
11. Bartley CM, Johns C, Ngo TT, et al. Anti-SARS-CoV-2 and autoantibody profiles in the cerebrospinal fluid of 3 teenaged patients with COVID-19 and subacute neuropsychiatric symptoms. *JAMA Neurol*. 2021;78:1503-1509. https://doi.org/10.1001/jamaneurol.2021.3821
12. Franke C, Ferse C, Kreye J, et al. High frequency of cerebrospinal fluid autoantibodies in COVID-19 patients with neurological symptoms. *Brain Behav Immun*. 2021;93:415-419. https://doi.org/10.1016/j.bbi.2020.12.022
13. Placantonakis DG, Aguero-Rosenfeld M, Flaifel A, et al. SARS-CoV-2 is not detected in the cerebrospinal fluid of encephalopathic COVID-19 patients. *Front Neurol*. 2020;11:587384. https://doi.org/10.3389/fneur.2020.587384
14. Zhang Y, Sun S, Du C, et al. Transmembrane serine protease TMPRSS2 implicated in SARS-CoV-2 infection is autoactivated intracellularly and requires N-glycosylation for regulation. *J Biol Chem*. 2022;298:102643. https://doi.org/10.1016/j.jbc.2022.102643
15. Fuentes-Prior P. Priming of SARS-CoV-2 S protein by several membrane-bound serine proteinases could explain enhanced viral infectivity and systemic COVID-19 infection. *J Biol Chem*. 2021;296:100135. https://doi.org/10.1074/jbc.REV120.015980
16. Kyrou I, Randeva HS, Spandidos DA, Karteris E. Not only ACE2-the quest for additional host cell mediators of SARS-CoV-2

infection: Neuropilin-1 (NRP1) as a novel SARS-CoV-2 host cell entry mediator implicated in COVID-19. *Signal Transduct Target Ther*. 2021;6:21. https://doi.org/10.1038/s41392-020-00460-9
17. Xia H, Lazartigues E. Angiotensin-converting enzyme 2: central regulator for cardiovascular function. *Curr Hypertens Rep*. 2010;12:170-175. https://doi.org/10.1007/s11906-010-0105-7
18. Daly JL, Simonetti B, Klein K, et al. Neuropilin-1 is a host factor for SARS-CoV-2 infection. *Science*. 2020;370:861-865. https://doi.org/10.1126/science.abd3072
19. Kong W, Montano M, Corley MJ, et al. Neuropilin-1 mediates SARS-CoV-2 infection of astrocytes in brain organoids, inducing inflammation leading to dysfunction and death of neurons. *mBio*. 2022;13:e0230822. https://doi.org/10.1128/mbio.02308-22
20. Gudowska-Sawczuk M, Mroczko B. The role of neuropilin-1 (NRP-1) in SARS-CoV-2 infection: review. *J Clin Med*. 2021;10:2772. https://doi.org/10.3390/jcm10132772
21. Li Y, Zhang Z, Yang L, et al. The MERS-CoV receptor DPP4 as a candidate binding target of the SARS-CoV-2 spike. *iScience*. 2020;23:101160. https://doi.org/10.1016/j.isci.2020.101160
22. Wang S, Qiu Z, Hou Y, et al. AXL is a candidate receptor for SARS-CoV-2 that promotes infection of pulmonary and bronchial epithelial cells. *Cell Res*. 2021;31:126-140. https://doi.org/10.1038/s41422-020-00460-y
23. Wang K, Chen W, Zhang Z, et al. CD147-spike protein is a novel route for SARS-CoV-2 infection to host cells. *Signal Transduct Target Ther*. 2020;5:283. https://doi.org/10.1038/s41392-020-00426-x
24. Jackson CB, Farzan M, Chen B, Choe H. Mechanisms of SARS-CoV-2 entry into cells. *Nat Rev Mol Cell Biol*. 2022;23:3-20. https://doi.org/10.1038/s41580-021-00418-x
25. Shin W-J, Ha DP, Machida K, Lee AS. The stress-inducible ER chaperone GRP78/BiP is upregulated during SARS-CoV-2 infection and acts as a pro-viral protein. *Nat Commun*. 2022;13:6551. https://doi.org/10.1038/s41467-022-34065-3
26. Shin J, Toyoda S, Fukuhara A, Shimomura I. GRP78, a novel host factor for SARS-CoV-2: the emerging roles in COVID-19 related to metabolic risk factors. *Biomedicines*. 2022;10:1995. https://doi.org/10.3390/biomedicines10081995
27. Offord C. MRI study charts organ damage months after COVID-19. *Science*. 2023;381:1385. https://doi.org/10.1126/science.adl0645
28. Yang AC, Kern F, Losada PM, et al. Dysregulation of brain and choroid plexus cell types in severe COVID-19. *Nature*. 2021;595:565-571. https://doi.org/10.1038/s41586-021-03710-0
29. Massimo M, Barelli C, Moreno C, et al. Haemorrhage of human foetal cortex associated with SARS-CoV-2 infection. *Brain*. 2023;146:1175-1185. https://doi.org/10.1093/brain/awac372
30. Lee M-H, Perl DP, Nair G, et al. Microvascular injury in the brains of patients with Covid-19. *N Engl J Med*. 2021;384:481-483. https://doi.org/10.1056/NEJMc2033369
31. Wenzel J, Lampe J, Müller-Fielitz H, et al. The SARS-CoV-2 main protease Mpro causes microvascular brain pathology by cleaving NEMO in brain endothelial cells. *Nat Neurosci*. 2021;24:1522-1533. https://doi.org/10.1038/s41593-021-00926-1
32. Pellegrini L, Albecka A, Mallery DL, et al. SARS-CoV-2 infects the brain choroid plexus and disrupts the blood-CSF barrier in human brain organoids. *Cell Stem Cell*. 2020;27:951-961.e5.e5. https://doi.org/10.1016/j.stem.2020.10.001
33. Jacob F, Pather SR, Huang W-K, et al. Human pluripotent stem cell-derived neural cells and brain organoids reveal SARS-CoV-2 neurotropism predominates in choroid plexus epithelium. *Cell Stem Cell*. 2020;27: 937-950.e9. https://doi.org/10.1016/j.stem.2020.09.016
34. Wang L, Sievert D, Clark AE, et al. A human three-dimensional neural-perivascular "assembloid" promotes astrocytic development and enables modeling of SARS-CoV-2 neuropathology. *Nat Med*. 2021;27:1600-1606. https://doi.org/10.1038/s41591-021-01443-1
35. Andrews MG, Mukhtar T, Eze UC, et al. Tropism of SARS-CoV-2 for human cortical astrocytes. *Proc Natl Acad Sci U S A*. 2022;119:e2122236119. https://doi.org/10.1073/pnas.2122236119
36. Kadoshima T, Sakaguchi H, Nakano T, et al. Self-organization of axial polarity, inside-out layer pattern, and species-specific progenitor dynamics in human ES cell-derived neocortex. *Proc Natl Acad Sci U S A*. 2013;110:20284-20289. https://doi.org/10.1073/pnas.1315710110
37. Spiteri G, Fielding J, Diercke M, et al. First cases of coronavirus disease 2019 (COVID-19) in the WHO European Region, 24 January to 21 February 2020. *Euro Surveill*. 2020;25:2000178. https://doi.org/10.2807/1560-7917.ES.2020.25.9.2000178
38. Xie X, Muruato A, Lokugamage KG, et al. An infectious cDNA clone of SARS-CoV-2. *Cell Host Microbe*. 2020;27:841841-848.e3.e3. https://doi.org/10.1016/j.chom.2020.04.004
39. Magni M, Bossi B, Conforti P, et al. Brain regional identity and cell type specificity landscape of human cortical organoid models. *Int J Mol Sci* . 2022;23:13159. https://doi.org/10.3390/ijms232113159
40. Zeng C, Evans JP, King T, et al. SARS-CoV-2 spreads through cell-to-cell transmission. *Proc Natl Acad Sci U S A*. 2022;119(1):119. https://doi.org/10.1073/pnas.2111400119
41. Torres-Fernández O, Yepes GE, Gómez JE, Pimienta HJ. Calbindin distribution in cortical and subcortical brain structures of normal and rabies-infected mice. *Int J Neurosci*. 2005;115:1375-1382. https://doi.org/10.1080/00207450590956396
42. Ye Z, Wong CK, Li P, Xie Y. A SARS-CoV protein, ORF-6, induces caspase-3 mediated, ER stress and JNK-dependent apoptosis. *Biochim Biophys Acta*. 2008;1780:1383-1387. https://doi.org/10.1016/j.bbagen.2008.07.009
43. Espuny-Camacho I, Arranz AM, Fiers M, et al. Hallmarks of Alzheimer's Disease in stem-cell-derived human neurons transplanted into mouse brain. *Neuron*. 2017;93: 1066-1081.e8. https://doi.org/10.1016/j.neuron.2017.02.001
44. Birey F, Andersen J, Makinson CD, et al. Assembly of functionally integrated human forebrain spheroids. *Nature*. 2017;545:54-59. https://doi.org/10.1038/nature22330
45. Bagley JA, Reumann D, Bian S, Lévi-Strauss J, Knoblich JA. Fused cerebral organoids model interactions between brain regions. *Nat Methods*. 2017;14:743-751. https://doi.org/10.1038/nmeth.4304
46. Xiang Y, Tanaka Y, Patterson B, et al. Fusion of regionally specified hPSC-derived organoids models human brain development and interneuron migration. *Cell Stem Cell*. 2017;21:383383-398.e7.e7. https://doi.org/10.1016/j.stem.2017.07.007
47. Xiang Y, Tanaka Y, Cakir B, et al. hESC-derived thalamic organoids form reciprocal projections when fused with cortical organoids. *Cell Stem Cell*. 2019;24:487-497.e7. https://doi.org/10.1016/j.stem.2018.12.015
48. Muguruma K, Nishiyama A, Kawakami H, Hashimoto K, Sasai Y. Self-organization of polarized cerebellar tissue in 3D culture of human pluripotent stem cells. *Cell Rep*. 2015;10:537-550. https://doi.org/10.1016/j.celrep.2014.12.051
49. Zamanian JL, Xu L, Foo LC, et al. Genomic analysis of reactive astrogliosis. *J Neurosci*. 2012;32:6391-6410. https://doi.org/10.1523/JNEUROSCI.6221-11.2012
50. Kim H, Leng K, Park J, et al. Reactive astrocytes transduce inflammation in a blood-brain barrier model through a TNF-STAT3 signaling axis and secretion of alpha 1-antichymotrypsin. *Nat Commun*. 2022;13:6581. https://doi.org/10.1038/s41467-022-34412-4
51. King A, Szekely B, Calapkulu E, et al. The increased densities, but different distributions, of both C3 and S100A10 immunopositive astrocyte-like cells in Alzheimer's Disease brains suggest possible roles for both A1 and A2 astrocytes in the disease pathogenesis. *Brain Sci*. 2020;10:503. https://doi.org/10.3390/brainsci10080503
52. Fan Y-Y, Huo J. A1/A2 astrocytes in central nervous system injuries and diseases: angels or devils? *Neurochem Int*. 2021;148:105080. https://doi.org/10.1016/j.neuint.2021.105080

53. Taha DM, Clarke BE, Hall CE, et al. Astrocytes display cell autonomous and diverse early reactive states in familial amyotrophic lateral sclerosis. *Brain*. 2022;145:481-489. https://doi.org/10.1093/brain/awab328
54. Prakash P, Erdjument-Bromge H, O'Dea MR, et al. Proteomic profiling of interferon-responsive reactive astrocytes in rodent and human. *Glia*. 2024;72:625-642. https://doi.org/10.1002/glia.24494
55. Wu P-T, Su W-R, Li C-L, et al. Inhibition of CD44 induces apoptosis, inflammation, and matrix metalloproteinase expression in tendinopathy. *J Biol Chem*. 2019;294:20177-20184. https://doi.org/10.1074/jbc.RA119.009675
56. Xiong X-Y, Tang Y, Yang Q-W. Metabolic changes favor the activity and heterogeneity of reactive astrocytes. *Trends Endocrinol Metab*. 2022;33:390-400. https://doi.org/10.1016/j.tem.2022.03.001
57. Izuo N, Nojiri H, Uchiyama S, et al. Brain-specific superoxide dismutase 2 deficiency causes perinatal death with spongiform encephalopathy in mice. *Oxid Med Cell Longev*. 2015;2015:238914. https://doi.org/10.1155/2015/238914
58. Weber S, Alpermann T, Dicker F, et al. BAALC expression: a suitable marker for prognostic risk stratification and detection of residual disease in cytogenetically normal acute myeloid leukemia. *Blood Cancer J*. 2014;4:e173. https://doi.org/10.1038/bcj.2013.71
59. Xu B, Chen G, Shi P, et al. shRNA-Mediated BAALC knockdown affects proliferation and apoptosis in human acute myeloid leukemia cells. *Hematol*. 2012;17:35-40. https://doi.org/10.1179/102453312X13221316477499
60. Xiao GH, Jeffers M, Bellacosa A, et al. Anti-apoptotic signaling by hepatocyte growth factor/Met via the phosphatidylinositol 3-kinase/Akt and mitogen-activated protein kinase pathways. *Proc Natl Acad Sci U S A*. 2001;98:247-252. https://doi.org/10.1073/pnas.98.1.247
61. Vivinetto AL, Kim I-D, Goldberg DC, et al. Zeb2 is a regulator of astrogliosis and functional recovery after CNS injury. *Cell Rep*. 2020;31:107834. https://doi.org/10.1016/j.celrep.2020.107834
62. Koper MJ, Vasn Schoor E, Ospitalieri S, et al. Necrosome complex detected in granulovacuolar degeneration is associated with neuronal loss in Alzheimer's disease. *Acta Neuropathol*. 2020;139:463-484. https://doi.org/10.1007/s00401-019-02103-y
63. Matschke J, Lütgehetmann M, Hagel C, et al. Neuropathology of patients with COVID-19 in Germany: a post-mortem case series. *Lancet Neurol*. 2020;19:919-929. https://doi.org/10.1016/S1474-4422(20)30308-2
64. Moriguchi T, Harii N, Goto J, et al. A first case of meningitis/encephalitis associated with SARS-Coronavirus-2. *Int J Infect Dis*. 2020;94:55-58. https://doi.org/10.1016/j.ijid.2020.03.062
65. Spudich S, Nath A. Nervous system consequences of COVID-19. *Science*. 2022;375:267-269. https://doi.org/10.1126/science.abm2052
66. Mesci P, de Souza JS, Martin-Sancho L, et al. SARS-CoV-2 infects human brain organoids causing cell death and loss of synapses that can be rescued by treatment with Sofosbuvir. *PLoS Biol*. 2022;20:e3001845. https://doi.org/10.1371/journal.pbio.3001845
67. Tiwari SK, Wang S, Smith D, Carlin AF, Rana TM. Revealing tissue-specific SARS-CoV-2 infection and host responses using human stem cell-derived lung and cerebral organoids. *Stem Cell Rep*. 2021;16:437-445. https://doi.org/10.1016/j.stemcr.2021.02.005
68. Song E, Zhang C, Israelow B, et al. Neuroinvasion of SARS-CoV-2 in human and mouse brain. *J Exp Med*. 2021;218:e20202135. https://doi.org/10.1084/jem.20202135
69. Ramani A, Pranty A-I, Gopalakrishnan J. Neurotropic effects of SARS-CoV-2 modeled by the human brain organoids. *Stem Cell Rep*. 2021;16:373-384. https://doi.org/10.1016/j.stemcr.2021.02.007
70. Zhang B-Z, Chu H, Han S, et al. SARS-CoV-2 infects human neural progenitor cells and brain organoids. *Cell Res*. 2020;30:928-931. https://doi.org/10.1038/s41422-020-0390-x
71. Wang C, Zhang M, Garcia G, et al. ApoE-isoform-dependent SARS-CoV-2 neurotropism and cellular response. *Cell Stem Cell*. 2021;28:331-342.e5. https://doi.org/10.1016/j.stem.2020.12.018
72. Oh J, Cho W-H, Barcelon E, et al. SARS-CoV-2 spike protein induces cognitive deficit and anxiety-like behavior in mouse via non-cell autonomous hippocampal neuronal death. *Sci Rep*. 2022;12:5496. https://doi.org/10.1038/s41598-022-09410-7
73. Beckman D, Bonillas A, Diniz GB, et al. SARS-CoV-2 infects neurons and induces neuroinflammation in a non-human primate model of COVID-19. *Cell Rep*. 2022;41:111573. https://doi.org/10.1016/j.celrep.2022.111573
74. Davis HE, McCorkell L, Vogel JM, Topol EJ. Long COVID: major findings, mechanisms and recommendations. *Nat Rev Microbiol*. 2023;21:133-146. https://doi.org/10.1038/s41579-022-00846-2
75. Walker KA, Chen J, Shi L, et al. Proteomics analysis of plasma from middle-aged adults identifies protein markers of dementia risk in later life. *Sci Transl Med*. 2023;15:eadf5681. https://doi.org/10.1126/scitranslmed.adf5681